

Observation of a Topological Transition in the Bulk of a Non-Hermitian System

Julia M. Zeuner,^{1,*} Mikael C. Rechtsman,^{2,†} Yonatan Plotnik,³ Yaakov Lumer,³ Stefan Nolte,¹ Mark S. Rudner,⁴ Mordechai Segev,³ and Alexander Szameit¹

¹*Institute of Applied Physics, Friedrich-Schiller-Universität Jena, Max-Wien-Platz 1, 07743 Jena, Germany*

²*Department of Physics, The Pennsylvania State University, University Park, Pennsylvania 16802, USA*

³*Department of Physics, Technion—Israel Institute of Technology, Haifa 32000, Israel*

⁴*The Niels Bohr International Academy, Niels Bohr Institute, 2100 Copenhagen, Denmark*

(Received 31 July 2014; revised manuscript received 24 February 2015; published 23 July 2015)

We present the first experimental observation of a topological transition in a non-Hermitian system. In contrast to standard methods for examining topological properties, which involve probing edge (or surface) states, we monitor the topological transition by employing bulk dynamics only. The system is composed of a lattice of evanescently coupled optical waveguides, and non-Hermitian behavior is engineered by inducing bending loss by spatially “wiggling” every second waveguide.

DOI: 10.1103/PhysRevLett.115.040402

PACS numbers: 03.65.Vf, 42.50.Ar, 42.82.Et

Topological transport was first proposed by Thouless, Kohmoto, Nightingale, and den Nijs [1], who showed that the Hall conductance of a two-dimensional electron gas is proportional to an integer-valued topological quantity. This introduces a striking robustness: small changes to the system (including disorder) have no effect [2]. Nontrivial topology implies conducting surface (or edge) states, which play a central role in many topological phenomena. A subsequent resurgence of interest in topological phenomena began with the prediction and observation of the quantum spin Hall effect [3–5], followed by the prediction [6,7] and observation [8] of an analogue of the quantum Hall effect for electromagnetic waves in the microwave regime. Proposals were subsequently put forward on how to achieve topologically protected optical transport [9–12] and experimentally realized by using waveguide arrays [13]. A different structure was used to implement this phenomenon in a silicon platform [14]. Recent progress demonstrated topological phenomena in ultracold gases, such as the measurement of the Zak phase [15]. However, in typical cold atom experiments, accessing edge physics is challenging, due to the smoothness of the magneto-optic trap [16]. Accordingly, measuring topological properties therein must be carried out by a complex procedure of sweeping the wave function through the Brillouin zone [17–21]. Similar ideas have been proposed for exciton-polariton systems [22], and a direct measurement of the Zak phase was suggested for a waveguide lattice [23].

Concurrently, notions of topological physics were introduced also in dissipative non-Hermitian systems [24–29]. Under appropriate conditions, the history of the wave function in a non-Hermitian system may encode topological features of the system’s band structure. Such features are reflected in robustly quantized values of certain observables [24]. This discovery is important, first because it identifies a methodology for unraveling the topological behavior of non-Hermitian systems. Second, it proposes a

way to study topological features by examining the history of the bulk wave function, something that would otherwise require complicated protocols [15,20] or probing edge physics [5,13,30].

Here, we present the first experiment to probe the topological properties of a non-Hermitian system. We show that its topological nature can be probed by bulk experiments.

We study an optical setup designed to realize the idealized one-dimensional (1D) non-Hermitian dimer model (NHDM) of [24]. The NHDM resembles the Su-Schrieffer-Heeger (SSH) model of polyacetylene [31], also called the dimer model, defined in terms of hopping on a 1D lattice with alternating strong and weak bonds. The SSH model features topologically distinct phases, corresponding to two inequivalent dimerization patterns. The NHDM contains an additional ingredient: particles can be lost or absorbed at every second site.

Our experimental system is based on the model in Ref. [24], originally conceived as a “quantum walk” in energy space, where levels are by nature *discrete*. We map this behavior to a continuous system: an array of coupled waveguides. In *continuous* periodic systems, such as crystalline materials, photonic crystals, waveguide arrays, or superconducting circuits, deviations from the idealized tight-binding description can be important. This is especially significant in non-Hermitian systems, where loss is added into the model phenomenologically, representing radiation-mode coupling. Furthermore, Hilbert space dimensionality plays a crucial role in defining the topology for the non-Hermitian system in Ref. [24], controlling the prevalence of “dark states” which mark the topological transition points. In particular, for a generic system with M sites per unit cell, nontrivial winding can occur only in the case where one site is lossy, while the remaining $M - 1$ sites are stable [32]. When more than one site per unit cell is lossy, dark states (i.e., eigenstates that avoid all lossy sites) become too rare to induce quantization. From this point of

view, it is an open question as to how predictions of Ref. [24] will hold in an experimental setting based on a continuous variable implementation.

We implement the NHDM in a photonic setting, although the concept is general. Our system is composed of an array of evanescently coupled waveguides [Fig. 1(a)]. The input facet is sketched in Fig. 1(b), labeling the sublattices A and B and cell index m [33]. The cell length is d , and the spacings between A and B sublattices are d_1 and d_2 , leading to a dimerization $\Delta d = (d_1 - d_2)/2$. Coupled optical systems are well suited to examining other non-Hermitian effects (such as parity-time symmetric systems) with the refractive index distribution as the real part of the potential and the gain and loss parameter as the imaginary part [34]. By oscillating every second waveguide, radiation loss is introduced [35,36]. Such a waveguide mimics a temporally oscillating potential well: oscillation introduces leakage to continuum modes. These modes radiate, never to return, leading to loss of the guided light. The notion of spatially oscillating waveguide channels to induce bending losses yields highly tunable non-Hermiticity, a technique that can be used broadly in other systems. The small wiggling is chosen transverse to the lattice plane to minimize the change of the distance between adjacent waveguides. Thus, to a good approximation, the coupling is time independent [35]. The full continuum description of the propagation of light therein is given by the paraxial approximation to Maxwell's equations, which is mathematically equivalent to the Schrödinger equation:

$$i\partial_z\psi(x,y,z) = -\frac{1}{2k_0}\nabla^2\psi(x,y,z) - \frac{k_0\Delta n(x,y,z)}{n_0}\psi(x,y,z), \quad (1)$$

where z represents the propagation distance along the waveguide axis, k_0 is the wave number of light in the medium, ∇^2 is in the transverse (x,y) plane, $\Delta n(x,y,z)$ is the refractive index change profile of the waveguides, and

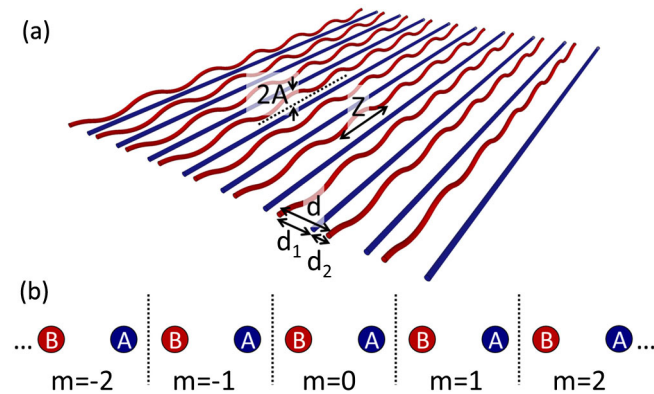


FIG. 1 (color online). (a) Schematic diagram of the waveguide array. The B sites oscillate in the vertical direction with a period $Z = 1$ mm, causing bending or radiation losses to continuum modes. (b) Sketch of the input facet labeling the unit cell index m and the sublattices A (nonlossy) and B (lossy).

n_0 represents the ambient refractive index. If $\Delta n(x,y,z)$ is real, then Eq. (1) is Hermitian (thus conservative); if the material has a spatially uniform absorption coefficient (always present but very small here), this causes an overall decay of the wave function as a function of z (but when this is factored out the propagation is still Hermitian). Desired loss is implemented by the aforementioned waveguide wiggling. Our system is equivalent to an open quantum system, which is also represented by a non-Hermitian model [37,38]. Solving Eq. (1) numerically in the continuum simulations, we use absorbing boundary conditions, forcing our system to be non-Hermitian [39].

The single-mode waveguides can be modeled by using tight-binding equations. This yields a discrete Schrödinger equation [43,44], with the distance along the waveguide axis, z , acting in place of time t :

$$i\partial_z \begin{pmatrix} a_m \\ b_m \end{pmatrix} = - \begin{pmatrix} c_1 b_m + c_2 b_{m-1} \\ c_1 a_m + c_2 a_{m+1} - i\gamma \frac{b_m}{2} \end{pmatrix}, \quad (2)$$

where c_1 and c_2 are coupling (hopping) constants between waveguides, and γ is the loss rate. The couplings are tuned by varying the spacing, and γ is tuned by varying the amplitude and period of the oscillation. In the basis of periodic Bloch functions, the Hamiltonian is given by

$$H(k) = - \begin{pmatrix} 0 & c_1 + c_2 e^{ik} \\ c_2 e^{-ik} + c_1 & -i\frac{\gamma}{2} \end{pmatrix}, \quad (3)$$

where k is the Bloch wave number. For $\gamma = 0$, this is precisely the SSH model. Therein, for any k , the Bloch eigenstates (viewed as a pseudospin) lie on the equator of the Bloch sphere. The topological number is the “winding number”: the number of loops made by a Bloch state around the equator of the Bloch sphere, as k passes through the Brillouin zone [15,45–47]. Here, the winding number w yields $|w| = 0$ or 1 , in the cases $c_1 > c_2$ and $c_1 < c_2$, respectively; a nonzero winding number is referred to as being “topologically nontrivial.” Here, the winding number is equivalent to the Zak phase [45,47], up to a factor of π . The bulk-edge correspondence principle [48] states that, at an interface between a topologically trivial and nontrivial crystal, a localized state forms. Typically, the topological nature of a system is probed via these edge states [5,13,30,49].

With nonzero loss, the NHDM presents a different paradigm of topology [24]. Here, a winding number is associated with the number of times the Bloch eigenstates encircle the polar axis of the Bloch sphere, independent of the presence of symmetry in the A and B sublattice potentials. The σ_z axis is special due to the existence of a nondecaying dark state that lives entirely on the A sublattice, at the north pole of the Bloch sphere. Note that *both* eigenstates of the Bloch Hamiltonian must avoid the north pole (i.e., the dark state) for all values of k . Both the

SSH and NHDM feature a transition of the topological number at exactly $c_1 = c_2$; in the case where A and B sublattice potentials are equal, the winding number of the NHDM coincides with that of the SSH model. Remarkably, within the NHDM, the expected mean displacement $\langle \Delta m \rangle$ achieved by a particle initialized on the nondecaying sublattice, is topologically quantized, with its value given by the winding number.

Under inversion, the waveguide structure with a given dimerization Δd maps to the structure with dimerization $-\Delta d$. This raises the question of how these two structures can have different winding numbers while having the same bulk structure. Here, symmetry is broken by the choice of the unit cell labeling—not by the edges. Thus, phases here cannot be labeled as topologically trivial ($w = 0$) or non-trivial ($w \neq 0$); what is important is only the distinction between phases: their differing winding numbers (see [15]). Therefore, the transition is a probe of the difference in the winding numbers in the phases of the NHDM.

We first examine the case where light is injected (at $z = 0$) with unit amplitude into the (nonlossy) A site of unit cell $m = 0$. The mean displacement is [24]

$$\langle \Delta m \rangle = \gamma \sum_m \int_0^\infty dz |\psi_m^{(B)}(z)|^2, \quad (4)$$

where $\psi_m^{(B)}(z)$ is the amplitude on site B of unit cell m at distance z . $\langle \Delta m \rangle$ depends upon the wave function's history. As shown in Ref. [24], $\langle \Delta m \rangle$ equals the winding number if the A site is excited. Figure 2 shows $\langle \Delta m \rangle$ as a function of the dimerization, obtained from tight-binding simulations for a large system size and long propagation length. The coupling function used in the simulations is $c(d) = 27.3/\text{cm} \cdot e^{(-0.195/\mu\text{m})d}$ (the decay factor is sufficiently large to neglect next-nearest-neighbor coupling). This dependence was obtained from light propagation experiments in two waveguides acting as a directional coupler. The two curves (blue and red) correspond to initialization on the A and B sublattices, respectively.

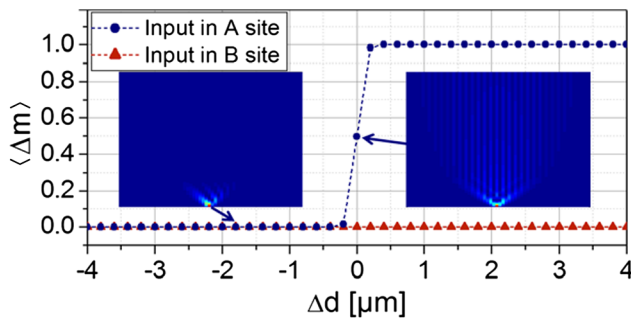


FIG. 2 (color online). Mean displacement $\langle \Delta m \rangle$ plotted as a function of Δd . The blue curve depicts the result when light is input in the A site, and the red curve corresponds to input at the B site. The insets show the absolute value of the wave function as a function of z (ascending) in the waveguide array (note the presence of the long-lived dark state on the right inset).

The transition from $\langle \Delta m \rangle = 0$ to $\langle \Delta m \rangle = 1$ at $\Delta d = 0$ is shown by the blue curve in Fig. 2, coinciding with the change of the winding number: the switching between different topological phases. When light is launched at a lossy B site, $\langle \Delta m \rangle$ is robustly quantized to zero, as seen in simulations (red curve) and hence, no transition takes place, and $\langle \Delta m \rangle$ remains zero for all Δd (see Sec. I in Ref. [39]). The z evolution is plotted in the insets in Fig. 2 for $\Delta d = 0$ (i.e., at the transition) and $\Delta d = 2.8 \mu\text{m}$ (away from it). Interestingly, despite the loss, the lifetime of the wave function diverges at $\Delta d = 0$ (Fig. 2, right inset); however, it is finite at $\Delta d = 2.8 \mu\text{m}$ (Fig. 2, left inset). This results from the dark state: a nondecaying eigenstate residing only on nonlossy sites [24,35]. It leads to a diverging variance $\langle \Delta m^2 \rangle$, which accompanies the jump in $\langle \Delta m \rangle$ and signals the topological transition.

We fabricate such lattices in fused silica glass by using femtosecond direct laser writing [50] with parameters described in Refs. [35,36]. Each lattice consists of 34 waveguides and is 10 cm long. The waveguides are arranged with alternating distances d_1 and d_2 (Fig. 1). To introduce loss, every second waveguide is sinusoidally oscillated as a function of z . The wiggling is transverse to the plane of the waveguides, with oscillation amplitude $A = 3 \mu\text{m}$ and period $Z = 1 \text{ mm}$, resulting in a loss factor $\gamma \approx 0.53/\text{cm}$. Every waveguide also contains a small intrinsic loss of $\gamma \approx 0.08/\text{cm}$, which can be factored out as it is identical in every site. These values were measured in isolated waveguides and fabricated with the same parameters. We implement 11 waveguide lattices with a lattice constant $d = 36 \mu\text{m}$, with different distances d_1 and d_2 , where $d_1 + d_2 = d$. In the most dimerized case, we use $|\Delta d| = 4 \mu\text{m}$, which is decreased in each subsequent array in steps of $0.4 \mu\text{m}$ to $\Delta d = 0$, corresponding to equally spaced waveguides. We excite a single waveguide in the central unit cell ($m = 0$) with laser light at $\lambda = 633 \text{ nm}$ and employ fluorescence microscopy [50,51] to observe the wave function intensity as a function of z . Hence, we compute $\langle \Delta m \rangle$ as defined in Eq. (4).

In Fig. 3, we plot the measured $\langle \Delta m \rangle$ as a function of Δd . We use the fact that two systems with the same $|\Delta d|$ are realized in the same sample, which just has to be inverted during data analysis. One can see a clear transition from $\langle \Delta m \rangle \sim 0$ to $\langle \Delta m \rangle \sim 0.82$ when a straight waveguide (A sublattice) in the central cell of the array ($m = 0$) is excited. In the case where the B site is excited, $\langle \Delta m \rangle$ shows small fluctuations around zero, coinciding with predictions in Fig. 2 (also, see Sec. I in Ref. [39]). Two examples of the fluorescence images for $\Delta d = 0$ and $\Delta d = 2.8 \mu\text{m}$ are shown in the insets in Fig. 3. Background noise is subtracted; however, there is inevitably some residual noise. Figure 3 shows the experimental results along with both continuum simulations and tight-binding simulations, which differ from those in Fig. 2 since here we use the parameters of the experimental system.

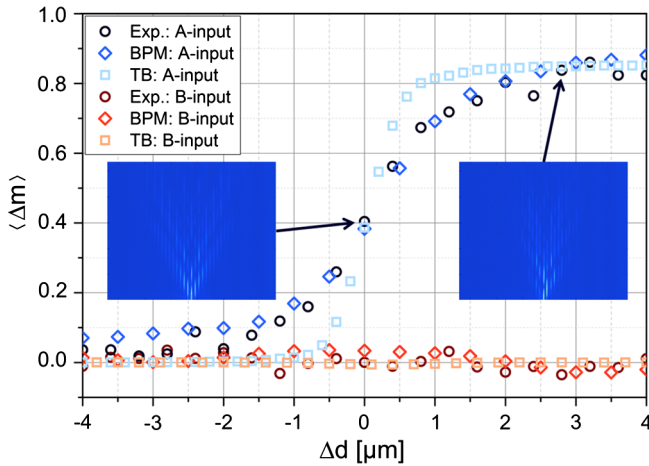


FIG. 3 (color online). Experimental and simulation results showing the mean displacement $\langle \Delta m \rangle$ vs Δd . The insets represent experimentally achieved fluorescence images. Blue shades correspond to injection on a nonlossy site, red shades on a lossy site.

In our experiment, we see the topological transition in our non-Hermitian system via a bulk measurement: the first observation of a dissipative topological transition. Of course, as for any continuous physical system, the transition is not as sharp as that predicted by the idealized tight-binding NHDM. The smoothness of the transition in the experiment and simulations (Fig. 3) can be attributed to (i) deviations from adiabaticity as the waveguides undergo oscillation to induce loss (indeed, continuum simulations show that propagation is not perfectly adiabatic at the 1 mm period), (ii) neglect of the overlap term between neighboring waveguide modes in the tight-binding approximation, (iii) the small overall loss being also present in the A-sites, and (iv) the fact that decay causes our experimental signal to get lost in noise for sufficiently large z —which effectively limits the length to which we can propagate. The last two points account for the deviation between the tight-binding simulations in Figs. 2 and 3. The differences between experiments and simulations may arise due to background radiation noise and deviations from a linear relationship between fluorescence and the light intensity. They do not arise from next-nearest-neighbor hopping, as this has no effect on the transition (unless the second-neighbor hopping becomes larger than the nearest-neighbor hopping—unphysical here). That said, the results match simulations and definitively show the transition. They also show no transition at all when the system is excited at the B site (as predicted). The agreement between theory, simulation, and experiment shows that the tight-binding model is a good approximation to the continuous problem and yields an accurate phenomenological description of the ultimately continuous system.

It is important to demonstrate the relevant topological edge physics here. When a system undergoes a transition from a topologically trivial to a nontrivial phase, edge states must emerge. We demonstrate this by launching light into

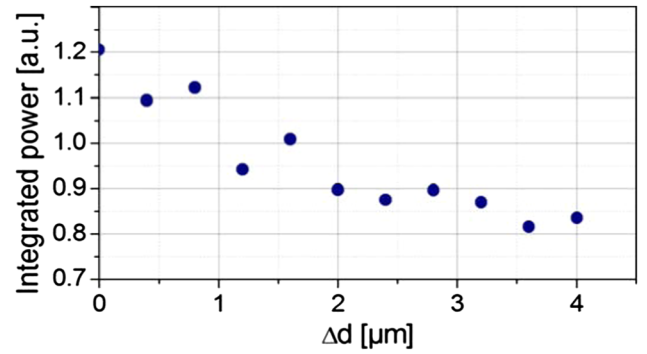


FIG. 4 (color online). Experimental results showing the total integrated power in all waveguides in the last 2.5 cm of propagation through the array, as a function of Δd .

the waveguides at the ends of our lattice. These experiments, shown in Sec. II in Ref. [39], clearly show confined edge states associated with a nonzero winding number. Monitoring the topological transition through the edge states confirms the findings we showed above extracted from bulk measurements.

Another prediction of Ref. [24] is that the lifetime of a walker in the bulk should diverge at the transition, here corresponding to $\Delta d = 0$, monotonically decreasing for increasing $|\Delta d|$. To investigate this, we plot the integrated power in the final quarter of the sample as a function of Δd (Fig. 4). We show only $\Delta d > 0$, as the inverted structures used to realize negative values of Δd yield identical results. Here, although we expect to have a maximum at the transition point ($\Delta d = 0$), we do not expect this quantity to diverge, because we are only measuring integrated power for a finite amount of propagation length z (indeed, true divergence is not physical for a finite sample length). Clearly, the remaining power reaches a maximum at the transition point, indicating that, for small dimerizations, the wave packet has the longest lifetime.

In conclusion, we have presented the first experimental observation of a topological transition in a non-Hermitian system; we do this by using bulk measurements. Our experiments show that the features of the idealized tight-binding model of Ref. [24] carry over to experiments. Indeed, loss is an inherent feature of many systems that may exhibit topological effects (such as coupled quantum dots [24], optical lattices [15], and driven-dissipative exciton-polariton condensates [52]). This non-Hermiticity may act as a surprising probe of their potentially rich topological phases.

The authors J. M. Z., S. N., and A. S. wish to thank the German Ministry of Education and Research (ZIK, Grant No. 03Z1HN31), the Deutsche Forschungsgemeinschaft (Grants No. NO462/6-1 and No. SZ276/7-1), and the German-Israeli Foundation for Scientific Research and Development (Grant No. 1157-127.14/2011). The work of M. C. R., Y. P., Y. L., and M. S. was supported by the ICORE Israeli Center of Excellence “Circle of Light”, the Israel Science Foundation, and the Binational USA-Israel

Science Foundation. M. R. acknowledges support from the Villum Foundation and the People Programme (Marie Curie Actions) of the European Union's Seventh Framework Programme (FP7/2007-2013) under REA Grant agreement No. PIFI-GA-2013-627838.

Julia M. Zeuner and Mikael C. Rechtsman contributed equally to this work.

*julia.zeuner@uni-jena.de
†mcrworld@psu.edu

- [1] D. J. Thouless, M. Kohmoto, M. P. Nightingale, and M. den Nijs, *Phys. Rev. Lett.* **49**, 405 (1982).
- [2] K. v. Klitzing, G. Dorda, and M. Pepper, *Phys. Rev. Lett.* **45**, 494 (1980).
- [3] C. L. Kane and E. J. Mele, *Phys. Rev. Lett.* **95**, 226801 (2005).
- [4] B. A. Bernevig, T. L. Hughes, and S.-C. Zhang, *Science* **314**, 1757 (2006).
- [5] M. König, S. Wiedmann, C. Brune, A. Roth, H. Buhmann, L. W. Molenkamp, X.-L. Qi, and S.-C. Zhang, *Science* **318**, 766 (2007).
- [6] F. D. M. Haldane and S. Raghu, *Phys. Rev. Lett.* **100**, 013904 (2008).
- [7] Z. Wang, Y. D. Chong, J. D. Joannopoulos, and M. Soljacic, *Phys. Rev. Lett.* **100**, 013905 (2008).
- [8] Z. Wang, Y. Chong, J. D. Joannopoulos, and M. Soljacic, *Nature (London)* **461**, 772 (2009).
- [9] R. O. Umucalılar and I. Carusotto, *Phys. Rev. A* **84**, 043804 (2011).
- [10] M. Hafezi, E. A. Demler, M. D. Lukin, and J. M. Taylor, *Nat. Phys.* **7**, 907 (2011).
- [11] K. Fang, Z. Yu, and S. Fan, *Nat. Photonics* **6**, 782 (2012).
- [12] A. B. Khanikaev, S. H. Mousavi, W.-K. Tse, M. Kargarian, A. H. MacDonald, and G. Shvets, *Nat. Mater.* **12**, 233 (2013).
- [13] M. C. Rechtsman, J. M. Zeuner, Y. Plotnik, Y. Lumer, D. Podolsky, F. Dreisow, S. Nolte, M. Segev, and A. Szameit, *Nature (London)* **496**, 196 (2013).
- [14] M. Hafezi, S. Mittal, J. Fan, A. Migdall, and J. M. Taylor, *Nat. Photonics* **7**, 1001 (2013).
- [15] M. Atala, M. Aidelsburger, J. T. Barreiro, D. Abanin, T. Kitagawa, E. Demler, and I. Bloch, *Nat. Phys.* **9**, 795 (2013).
- [16] A. L. Gaunt, T. F. Schmidutz, I. Gotlibovych, R. P. Smith, and Z. Hadzibabic, *Phys. Rev. Lett.* **110**, 200406 (2013).
- [17] D. A. Abanin, T. Kitagawa, I. Bloch, and E. Demler, *Phys. Rev. Lett.* **110**, 165304 (2013).
- [18] X.-J. Liu, K. T. Law, T. K. Ng, and P. A. Lee, *Phys. Rev. Lett.* **111**, 120402 (2013).
- [19] A. Dauphin and N. Goldman, *Phys. Rev. Lett.* **111**, 135302 (2013).
- [20] G. Jotzu, M. Messer, R. Desbuquois, M. Lebrat, T. Uehlinger, D. Greif, and T. Esslinger, *Nature (London)* **515**, 237 (2014).
- [21] M. Aidelsburger *et al.*, *Nat. Phys.* (to be published).
- [22] T. Ozawa and I. Carusotto, *Phys. Rev. Lett.* **112**, 133902 (2014).
- [23] S. Longhi, *Opt. Lett.* **38**, 3716 (2013).
- [24] M. S. Rudner and L. S. Levitov, *Phys. Rev. Lett.* **102**, 065703 (2009).
- [25] S. Diehl, E. Rico, M. A. Baranov, and P. Zoller, *Nat. Phys.* **7**, 971 (2011).
- [26] C.-E. Bardyn, M. A. Baranov, C. V. Kraus, E. Rico, A. İmamoğlu, P. Zoller, and S. Diehl, *New J. Phys.* **15**, 085001 (2013).
- [27] K. Esaki, M. Sato, K. Hasebe, and M. Kohmoto, *Phys. Rev. B* **84**, 205128 (2011).
- [28] H. Schomerus, *Opt. Lett.* **38**, 1912 (2013).
- [29] C. Yuce, *Phys. Lett. A* **379**, 1213 (2015).
- [30] D. Hsieh, D. Qian, L. Wray, Y. Xia, Y. S. Hor, R. J. Cava, and M. Z. Hasan, *Nature (London)* **452**, 970 (2008).
- [31] W. P. Su, J. R. Schrieffer, and A. J. Heeger, *Phys. Rev. Lett.* **42**, 1698 (1979).
- [32] M. Rudner *et al.* (to be published).
- [33] N. Malkova, I. Hromada, X. Wang, G. Bryant, and Z. Chen, *Opt. Lett.* **34**, 1633 (2009).
- [34] R. El-Ganainy, K. G. Makris, D. N. Christodoulides, and Z. H. Musslimani, *Opt. Lett.* **32**, 2632 (2007).
- [35] T. Eichelkraut, R. Heilmann, S. Weimann, S. Stützer, F. Dreisow, D. N. Christodoulides, S. Nolte, and A. Szameit, *Nat. Commun.* **4**, 2533 (2013).
- [36] T. Eichelkraut, S. Weimann, S. Stützer, S. Nolte, and A. Szameit, *Opt. Lett.* **39**, 6831 (2014).
- [37] L. D. Landau and E. M. Lifshits, *Quantum Mechanics: Non-relativistic Theory* (Butterworth-Heinemann, London, 1977).
- [38] N. Moiseyev, *Non-Hermitian Quantum Mechanics* (Cambridge University Press, Cambridge, England, 2011).
- [39] See Supplemental Material at <http://link.aps.org/supplemental/10.1103/PhysRevLett.115.040402> for more detailed information about continuum simulations, injection of light into B-site, and the observation of edge behaviour, which includes Refs. [40–42].
- [40] S. Ryu and Y. Hatsugai, *Phys. Rev. Lett.* **89**, 077002 (2002).
- [41] K. Kawano and T. Kitoh, *Introduction to Optical Waveguide Analysis: Solving Maxwell's Equation and the Schrödinger Equation* (Wiley, New York, 2001).
- [42] R. Kosloff and D. Kosloff, *J. Comput. Phys.* **63**, 363 (1986).
- [43] F. Lederer, G. I. Stegeman, D. N. Christodoulides, G. Assanto, M. Segev, and Y. Silberberg, *Phys. Rep.* **463**, 1 (2008).
- [44] A. L. Jones, *J. Opt. Soc. Am.* **55**, 261 (1965).
- [45] B. A. Bernevig and T. L. Hughes, *Topological Insulators and Topological Superconductors* (Princeton University Press, Princeton, NJ, 2013).
- [46] P. Delplace, D. Ullmo, and G. Montambaux, *Phys. Rev. B* **84**, 195452 (2011).
- [47] J. Zak, *Phys. Rev. Lett.* **62**, 2747 (1989).
- [48] S. Ryu and Y. Hatsugai, *Physica E (Amsterdam)* **22**, 679 (2004).
- [49] T. Kitagawa, M. A. Broome, A. Fedrizzi, M. S. Rudner, E. Berg, I. Kassal, A. Aspuru-Guzik, E. Demler, and A. G. White, *Nat. Commun.* **3**, 882 (2012).
- [50] A. Szameit and S. Nolte, *J. Phys. B* **43**, 163001 (2010).
- [51] A. Szameit, F. Dreisow, H. Hartung, S. Nolte, A. Tünnermann, and F. Lederer, *Appl. Phys. Lett.* **90**, 241113 (2007).
- [52] T. Jacqmin, I. Carusotto, I. Sagnes, M. Abbarchi, D. D. Solnyshkov, G. Malpuech, E. Galopin, A. Lemaître, J. Bloch, and A. Amo, *Phys. Rev. Lett.* **112**, 116402 (2014).